Journal of the Neurological Sciences 401 (2019) 19–26

Contents lists available at ScienceDirect

Journal of the Neurological Sciences

journal homepage: www.elsevier.com/locate/jns

Differential diagnosis of multiple system atrophy with predominant parkinsonism and Parkinson's disease using neural networks

Mitsunori Tsuda[a,*], Shingo Asano[a], Yasushi Kato[b], Katsumasa Murai[c], Masao Miyazaki[b]

[a] Neurology Tsuda Clinic, 3006 Hisaishinmachi, Tsu, Mie Prefecture 514-1118, Japan
[b] Neurology Kato Clinic, 4-5-36 Ichinoki, Ise City, Mie Prefecture 516-0071, Japan
[c] Neurology Kashou-kai, 234-10 Kamata-machi, Matsuzaka City, Mie Prefecture 515-0005, Japan

ARTICLE INFO

Keywords:
Neural network
Deep learning
Multiple system atrophy
Parkinson's disease
Voxel-based morphometry
Magnetic resonance spectroscopy

ABSTRACT

Differential diagnosis between Parkinson's disease (PD) and atypical parkinsonism, such as multiple system atrophy (MSA), can be difficult, especially in the early stages of the disease. Deep learning using neural networks (NNs) makes possible the prediction of the diagnosis using various types of biomarkers, unlike conventional linear statistics. We aimed to differentiate the Parkinson's variant of MSA (MSA-P) from PD both in the early stages by clinical utilization of NN analyses before the hot cross-bun and putaminal rim imaging features of MSA appeared. Analysis by NN involved the data of voxel-based morphometry (VBM) that indicate morphological changes and magnetic resonance spectroscopy (MRS) that indicate qualitative changes. VBM analysis showed that compared with PD patients, MSA-P patients showed atrophy in the superior cerebellar peduncle, middle cerebellar peduncle, cerebellar hemisphere, pons, midbrain, and putamen, but not in the globus pallidus. Proton MRS on the globus pallidus in the diseased hemisphere, lacking atrophy as observed with VBM, revealed decreased neurons and gliosis in both groups. Clinical differentiation of MSA-P from PD using NN analysis, involved measuring the prediction potential using the area under the receiver operator characteristic (ROC) curves (AUC). Using both VBM and MRS data, NNs contributed adequately to the clinical diagnosis.

1. Introduction

Differentiating between multiple system atrophy with predominant parkinsonism (MSA-P) and Parkinson's disease (PD) is often difficult. However, such differentiation is important for prognosis and treatment. Diagnostic accuracy of multiple system atrophy (MSA) varies greatly between different centers from as little as 29% up to 86% (approximately 62% according to autopsies), despite well-established diagnostic criteria [1–5]. Imaging techniques and biomarkers are urgently needed to improve the accuracy of in vivo clinical diagnosis. Various magnetic resonance imaging (MRI) techniques have been used for the differential diagnosis of atypical parkinsonism, such as MSA-P, and PD [6,7]. These findings suggest that better and novel MRI techniques are needed to improve the sensitivity, and to be able to serve as specific biomarkers for monitoring disease progression [1]. If the various MRI biomarkers are combined, a more comprehensive and more accurate diagnosis may be realized. To achieve this, a neural network (NN) approach, a type of deep learning is used. NN mainly makes possible the prediction of the diagnosis from various types of biomarkers unlike conventional linear statistics [8]. With regard to the data used for NN diagnosis of MSA-P, we examined morphological changes using voxel-based morphometry (VBM) [9] and qualitative changes in the intracellular metabolic status using magnetic resonance spectroscopy (MRS) [10,11]. Further, we aimed at differential diagnosis between MSA-P and PD in the earlier stages when the conventional MR imaging features of MSA namely, the putaminal rim sign, middle cerebellar peduncle sign, and hot cross-bun sign [2] have not appeared. In this study, we used only objective MRI data, without including the clinical findings, as the data of NN, because when the NN diagnosis is different from the clinical diagnosis, the results of NN can be used as a feedback to review the clinical diagnosis and neurological findings. This pilot study will be the first trial using NN in these neurological diseases.

2. Materials and methods

2.1. Patients

The subjects included patients with MSA-P ($n = 30$; mean ± SD [SD: standard deviation] age: 66.7 ± 4.2 years; 14 women and 16 men) and PD patients (n = 30; mean age: 66.8 ± 6.3 years; 18 women

* Corresponding author.
E-mail address: tsuda-mi@ruby.plala.or.jp (M. Tsuda).

https://doi.org/10.1016/j.jns.2019.04.014
Received 31 July 2018; Received in revised form 18 March 2019; Accepted 9 April 2019
Available online 11 April 2019
0022-510X/

Table 1
Demographic characteristics of MSA-P, PD, and controls.

Characteristics	MSA-P	PD	Controls
Ages (years)	66.7 ± 4.2 women 14, men 16	66.8 ± 6.3 women 18, men 12	66.8 ± 7.4 women 18, men 7
Diagnosis			
UMSARS-II	26.2 ± 3.4		
UPDRS-III	18.5 ± 3.9 Possible 28, probable 2	21.8 ± 5.6 H&Y II22,III8	
Disease duration (years)	2.7 ± 1.6	3.6 ± 2.5	
Parkinsonism	all present	all present	
Cerebellar symptoms	7 present, 23 absent		
Autonomic dysfunction	18 present, 12 absent		
Pyramidal signs	5 present, 25 absent		

MSA-P, multiple system atrophy - parkinsonian type; PD, Parkinson's disease; SD, standard deviation; The data indicate the means ± standard deviation. Controls of an age and sex-matched group are used in voxel-based morphometry (VBM) studies. The diagnosis of MSA-P was made based on UMSARS (unified MSA rating scale) Part II and the new diagnostic criteria (2nd consensus criteria) of multiple system atrophy.
The diagnosis of PD was made based on UPDRS-III, Unified Parkinson's and H&Y indicate Hoehn & Yahr Staging.

Table 2
The z-scores obtained from VBM of MSA-P compared to PD.

Area	*p* Value	z Scores[a]
Superior cerebellar peduncle	0.0001 >	Increase
Middle cerebellar peduncle	0.0001 >	Increase
Cerebellar hemisphere1[b]	0.0001 >	Increase
Cerebellar hemisphere2[c]	0.0001 >	Increase
Pallidum	0.5301	N.S.[d]
Putamen	0.0396	Increase
Pons	0.0001	Increase
Midbrain	0.0084	Increase

[a] The increase of z scores indicate the atropy of each area.
[b] Cerebellar hemisphere1 (the mean of MNI cerebellumI~VI).
[c] Cerebellar hemisphere 2 (the mean of MNI cerebellumVII~X).
[d] N.S. is no significant differences between the two groups.

and 12 men) and controls, an age and sex-matched group (n = 25; mean age: 66.8 ± 7.4 years; 18 women and 7 men). MSA-P and PD cases at earlier stage of the disease were chosen from our database and were diagnosed by two different neurologists (M.T^$(and M.M), twice, as reliable diagnosis was important for providing appropriate learning data to NN. The clinical diagnosis of MSA-P was made based on the unified MSA rating scale (UMSARS-II) [12] and the new diagnostic criteria (second consensus criteria) of MSA [5]. The clinical diagnosis of PD was made based on the motor subsection of the Unified Parkinson's Disease Rating Scale Part III (UPDRS-III) [13] and Hoehn and Yahr Staging (H&Y) [14].

In the MSA-P cases, the mean of UMSARS-II score was 26.2 ± 3.4 and the clinical diagnosis were almost possible MSA-P (possible 28 cases and probable 2 cases). In the PD cases, the mean UPDRS stage 2H &Y and 8 patients in stage 3H&Y. The patient profile including clinical features is indicated in Table 1.

All procedures followed were in accordance with the Declaration of Helsinki and investigations were performed with the approval of the Medical Communities Ethics Committee (Japanese local committee). The ethical approval number is 1(15th June 2018 accepted). Informed consent was obtained from all the patients.

2.2. Statistical analysis

The normality of all data in each group was confirmed using the chi-square test, and then Student's *t*-tests were performed for comparisons. *P*-values were based on the 2-sided tests and considered statistically significant at $P < 0.05$. The software used was the BellCurve for Excel (Social Survey Research Information Co., Ltd., Tokyo, Japan).

2.3. Voxel-based morphometry

For VBM, brain imaging data sequences were analyzed using Statistical Parametric Mapping (SPM12, v.12; Welcome Department of Cognitive Neurology, London, UK, http://www.fil.ion.ucl.ac.uk/spm/). For anatomical segmentation, Automated Anatomical Labeling (AAL) was used prior to determining the z-scores, which indicated the atrophy rate for each region of interest. A z-score of 1 represents 1 unit of standard deviation. MNI templates, created by the Montreal Neurological Institute (MNI), were used for all analyses. MNI templates are the anatomically segmented, spatially normalized single-subject high-resolution T1 volumes [15]. The regions examined in MSA-P and PD patients included the superior cerebellar peduncle, middle cerebellar peduncle, cerebellum hemisphere 1 (the mean of MNI cerebellum I~VI), cerebellum hemisphere 2 (the mean of MNI cerebellum VII~X), globus pallidus, putamen, pons, and midbrain.

2.4. Magnetic resonance spectroscopy

MRS (magnetic field strength: 1.5 T) was performed, using Proton MRS (^{1}HMRS), on the globus pallidus of the diseased hemisphere in which atrophy was not observed with VBM. We selected the globus pallidus for MRS as the region of interest because it has been reported that important changes occur in the globus pallidus during the early stage of PD [16,17]. We measured levels of lactate (Lac), *N*-acetylaspartate (NAA), gamma-aminobutyric acid (GABA), creatine + phosphocreatine (Cr), choline-containing compounds (Cho), and myoinositol (mI). Furthermore, we compared NAA with Cr (NAA/Cr), Cho with Cr (Cho/Cr), NAA with Cho (NAA/Cho), mI with Cr (mI/Cr), GABA with Cr (GABA/Cr), GABA with NAA (GABA/NAA), and GABA with mI (GABA/mI) in the globus pallidus of PD patients [18] as was described in our previous report. These values were obtained by approximating relative peak areas to the Lorentzian function.

2.5. Data analyses by the neural network

We used a stochastic NN as the NN for our analyses [19]. The NeuralTools 7.5 (Palisade Corporation, Ithaca, NY, USA) software was used. It was necessary to carefully select the data for learning of NNs. We examined all variable factors in the NNs and excluded the factors with a low contribution to the results. For the analysis of NNs, the z-values were selected from the areas in the superior cerebellar peduncle, middle cerebellar peduncle, cerebellum hemisphere 1, cerebellum hemisphere 2, globus pallidus, putamen, pons, and midbrain that were obtained using VBM and the peak area values of NAA/Cr, Cho/Cr,

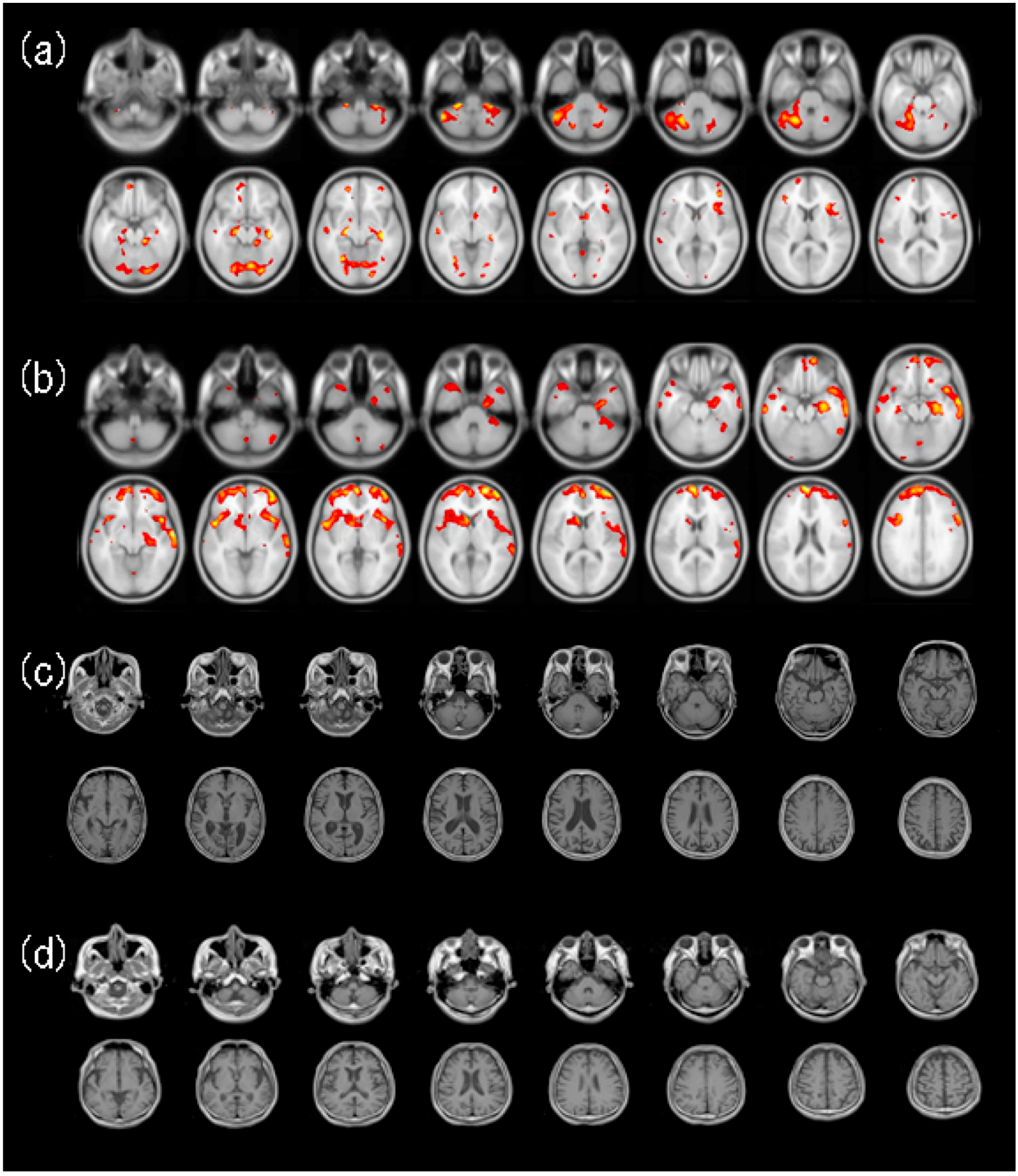

Fig. 1. Representative axial images obtained using VBM (SPM 12) and raw T1- weighted images (a) Parkinson's variant of multiple system atrophy (MSA-P), (b) Parkinson's disease (PD), (c) raw T1-weighted images of the MSA-P patient in (a), (d) raw T1- weighted image of the PD patient in (b). The colors red and yellow indicate atrophy of 2 standard deviations or more in the T1 weighted images. No significant differences were observed in the raw T1-weighted images in MSA-P and PD patients using visual image inspection alone, unless the VBM method was used. (For interpretation of the references to colour in this figure legend, the reader is referred to the web version of this article.)

NAA/Cho, mI/Cr, GABA/Cr, GABA/NAA, and GABA/mI that were obtained using MRS. These values were processed for the input layer as independent variables. The intermediate layer was set with 5 nodes for learning. The dependent variables (prediction values) were a diagnosis of either MSA-P, PD, or normal.

As the learning data of the NNs, 10 MSA-P (all possible MSA-P), 10

Table 3
The basic statistics of various parameters of metabolites obtained from MRS of MSA-P and PD.

(a) MSA to control[a]			(b) PD to control			(c) MSA to PD		
Metabolites	p Value	inc/dec	Metabolites	p Value	inc/dec	Metabolites	p Value	inc/dec
Lac	0.0477	Increase	Lac	0.0260	Increase	Lac	0.4311	N.S.
NAA	0.0010	Decrease	NAA	0.0220	Decrease	NAA	0.0890	N.S.
GABA	0.0269	Increase	GABA	0.0050	Increase	GABA	0.9956	N.S.
Cr	0.0120	Decrease	Cr	0.2590	N.S.	Cr	0.2768	N.S.
Cho	0.1100	N.S.	Cho	0.5380	N.S.	Cho	0.6726	N.S.
ml	0.0136	Increase	ml	0.0130	Increase	ml	0.5025	N.S.
NAA/Cr	0.0000	Decrease	NAA/Cr	0.0002	Decrease	NAA/Cr	0.1850	N.S.
Cho/Cr	0.8937	N.S.	Cho/Cr	0.0020	Decrease	Cho/Cr	0.5187	N.S.
NAA/Cho	0.2784	N.S.	NAA/Cho	0.3220	N.S.	NAA/Cho	0.8157	N.S.
ml/Cr	0.0044	Increase	ml/Cr	0.0230	Increase	ml/Cr	0.9114	N.S.
GABA/Cr	0.0079	Increase	GABA/Cr	0.0240	Increase	GABA/Cr	0.0777	N.S.
GABA/NAA	0.0210	Increase	GABA/NAA	0.0000	Increase	GABA/NAA	0.0709	N.S.
GABA/ml	0.6745	N.S.	GABA/ml	0.1960	N.S.	GABA/ml	0.5145	N.S.

MRS: magnetic resonance spectroscopy; MSA-P: Parkinson's variant of multiple system atrophy; PD: Parkinson's disease; Lac, lactate; NAA, *N*-acetylaspartate; GABA, gamma-aminobutyric acid; Cr, creatine + phosphocreatine; Cho, choline-containing compounds; mI, myoinositol.
[a] N.S.: no significant differences between the two groups.

Table 4
The values of area under the curve (AUC) obtained from Receiver Operating Characteristic (ROC) analysis.

Kind of NN	AUC	Values	*P* Values
VBM- NN[b]	0.6292	2.0311	0.1541
MRS-NN[c]	0.5217	0.0513	0.8209
VBM- and MRS-NN[d]	0.7749	12.3854	0.0004[a]

[a] $P < 0.01$ chi-square test (Null hypothesis:area = 0.5).
[b] VBM-NN: neuralnet was made with the only data of VBM.
[c] MRS-NN: neuralnet was made with the only data of MRS.
[d] VBM- and MRS-NN: neuralnet was made with the data of both VBM and MRS.

PD (all H&Y staging II) patients, and 5 normal individuals were selected. Thereafter, the learning effect of NNs was compared and examined in 20 MSA-P, 20 PD patients, and 20 normal persons. Three kinds of NNs were examined. The first NN was made with only the data of MRS (MRS-NN), the second NN (VBM-NN) was made with only the data of VBM, and, the third NN was made with all the data, of VBM and MRS (VBM and MRS-NN), to compare the accuracy of the NNs. The probability of prediction could be obtained from the NNs. The accuracy of each NN was evaluated by the values of area under the curve (AUC) obtained from Receiver Operating Characteristic (ROC) analysis using the values of probability [20].

3. Results

3.1. Voxel-based morphometry

Considering the z-scores in the VBM results revealed atrophy in the superior cerebellar peduncle, middle cerebellar peduncle, cerebellar hemisphere 1, cerebellar hemisphere 2, putamen, pons, and midbrain, and in the MSA-P patients when compared with PD patients, however, no significant difference was seen in the globus pallidus (Table 2: Fig. 1a, b. We did not find any significant difference in conventional MRI images between MSA-P and PD patients with visual image inspection alone, if the VBM method was not used (Fig. 1c, d).

The UMSARS-II scores were not significantly correlated except for the cerebellar hemisphere region. The correlation coefficients of cerebellar hemisphere 1 (the mean of MNI cerebellum I~VI) and cerebellar hemisphere 2 (the mean of MNI cerebellum VII~X) were $\rho = 0.788$ (95% credible interval 0.49%–0.92%) and $\rho = 0.752$ (95% credible interval 0.42%–0.91%) respectively.

3.2. Magnetic resonance spectroscopy

Table 3 outlines the results for various metabolic parameters in MSA-P and PD patients. In MSA-P patients, Lac, GABA, mI, mI/Cr, GABA/Cr, and GABA/NAA levels were increased, whereas NAA, Cr, and NAA/Cr levels were decreased in comparison with those of controls (Table 3a). In PD patients, Lac, GABA, mI, mI/Cr, GABA/Cr, and GABA/NAA levels were increased in comparison with controls, but NAA, NAA/Cr, and Cho/Cr levels were decreased in comparison with controls in globus pallidus of PD patients, as was described in our previous report [18] (Table 3b). However, no significant differences were found in the various metabolite parameters between MSA-P patients and PD patients (Table 3c). The UMSARS-II scores were not significantly correlated in all results.

3.3. Data analysis using neural networks

At first, we attempted to differentiate between MSA-P and PD using only MRS data in the MRS-NN; however, our results were unsatisfactory. Next, we attempted the same trial with only VBM data in the VBM-NN. The results were slightly improved; however, they were of low accuracy. However, on including both VBM data and MRS data (VBM- and MRS-NN), the accuracy of NNs to differentiate MSA-P from PD was fairly improved. In the Table 4, the values of AUC obtained by NNs were 0.775 (VBM and MRS-NNs), 0.625 (VBM-NN), and 0.522 (MRS-NN). The Receiver Operating Characteristic (ROC) curves obtained from neural networks are shown in Supplementary Fig. 1.

An example of the use of NN for the discrimination is shown in Table 5.

4. Discussion

Differential diagnosis between MSA-P and PD is often difficult. However, such differentiation is important for prognosis and treatment. Diagnostic accuracy in MSA varies greatly between different centers from as little as 29% up to 86% (approximately 62% according to autopsies), despite well-established diagnostic criteria [1–5]. The large difference in diagnostic accuracy may be due to the duration and stage of MSA and due to the presence of various pathological changes in MSA-P [21–23].

MRI has undoubtedly enhanced the accuracy of the differential diagnosis of MSA. The hyperintense putaminal rim, middle cerebellar

Table 5
Representation of Parkinson's variant of multiple system atrophy (MSA-P) prediction using neural network.

1HMRS							VBM z value			
NAA/Cr	Cho/Cr	NAA/Cho	ml/Cr	GABA/Cr	GABA/NAA	GABA/ml	Superior cerebellar peduncle_L	Superior cerebellar peduncle_R	Mid_cereb_peduncle_L	Mid_cereb_peduncle_R
1.79	0.9	1.982	0.04	0.088	0.05	2.244	0.256	0.219	0.265	0.448
0.165	0.991	2.518	0.084	0.187	0.075	2.222	−1.221	−0.624	2.082	1.603
0.127	0.975	4.382	0.278	0.246	0.058	0.886	0.393	0.883	0.586	0.818
2.268	9.838	0.723	0.595	0.76	0.107	1.276	1.871	2.579	2.263	2.448
1.952	4.193	1.226	0.971	1.969	0.383	2.027	2.62	3.818	2.685	2.182
0.048	0.324	5.133	0.68	0.527	0.317	0.775	3.302	3.81	3.176	2.901
2.46	1.52	1.62	0.146	0.211	0.086	1.441	1.039	1	0.996	0.851
0.05	1.335	1.579	0.075	0.052	0.025	0.687	1.545	1.794	2.097	1.776
0.309	0.448	7.889	0.668	1.399	0.396	2.093	1.857	2.348	2.069	2.438
0.055	0.768	1.851	0.156	0.134	0.094	0.858	0.838	0.821	0.633	0.961
0.117	1.426	1.291	0.137	0.923	0.502	6.736	0.396	0.846	0.906	1.79
0.067	1.326	0.988	0.153	0.166	0.127	1.084	0.302	0.974	1.105	0.444
0.059	0.257	0.541	0.377	0.351	2.528	0.932	0.787	1.967	3.052	2.55
0.246	2.048	4.294	0.411	0.645	0.073	1.568	1.163	1.306	0.711	1.217
0.329	10.713	2.439	1.29	0.449	0.017	0.348	0.737	0.538	0.994	0.34
0.727	2.889	1.951	0.968	0.74	0.131	0.764	1.781	1.653	1.476	1.227
0.074	1.202	1.753	0.097	0.133	0.063	1.37	0.504	0.428	0.487	0.378
0.095	1.538	1.37	0.245	0.201	0.095	0.821	1.068	0.939	1.547	1.246
0.072	1.54	1.433	0.296	0.203	0.092	0.685	2.565	2.497	0.618	1.208
1.017	7.741	0.043	1.784	0.313	0.935	0.175	0.466	0.968	0.767	0.836
0.068	2.067	1.262	0.628	0.189	0.072	0.301	0.706	1.327	0.613	0.164
0.223	0.754	1.434	0.186	0.132	0.122	0.709	0.771	0.734	1.24	1.3
0.113	2.616	1.234	0.02	0.257	0.08	12.917	−0.652	−0.736	−0.071	0.065
0.075	1.108	1.777	0.109	0.188	0.095	1.727	0.821	0.863	1.063	0.84
0.063	1.678	1.601	0.151	0.201	0.075	1.331	0.576	1.328	1.693	1.289
0.035	0.599	3.099	0.042	0.25	0.135	5.986	1.186	1.04	0.744	0.384
0.048	1.808	1.509	0.096	0.213	0.078	2.225	2.142	2.003	0.526	0.176
0.154	1.498	1.072	0.138	0.13	0.081	0.939	1.518	−0.51	1.585	2.212
0.132	1.172	2.097	0.141	0.099	0.04	0.702	−0.038	0.085	3.894	4.325
1.31	0.403	3.262	0.292	0.022	0.017	0.076	−1.043	−1.87	0.459	1.083
0.056	0.967	1.643	0.013	0.159	0.1	11.914	0.519	0.162	1.51	1.839
0.068	0.932	1.485	0.138	0.136	0.098	0.987	0.212	−0.339	1.346	1.416
2.08	1.555	1.338	0.28	0.335	0.161	1.197	0.673	0.406	1.293	1.747
0.172	1.197	4.087	0.185	0.009	0.002	0.05	−0.462	−0.279	1.549	1.992
0.297	5.91	1.46	0.323	0.597	0.069	1.849	−0.005	−0.0673	1.493	1.581
0.101	1.577	1.82	0.131	0.158	0.055	1.201	−0.138	−0.353	3.453	3.363
0.097	2.567	1.157	0.346	0.494	0.166	1.427	−0.733	−1.229	1.707	1.568

1HMRS	VBM z value									
NAA/Cr	cerebellum hemisphere1	cerebellum hemisphere2	MNI_Putamen_L	MNI_Putamen_R	Pons	Midbrain	Diagnosis		Prediction	Prediction %
1.79	2.401	2.388	−0.888	−1.232	1.051	1.076	MSA-P	Learning		
0.165	2.58	1.736	−0.055	−0.238	2.557	−0.177	MSA-P	Learning		
0.127	1.634	2.028	0.456	0.524	0.948	1.149	MSA-P	Learning		
2.268	2.282	2.7	3.476	2.146	2.658	2.83	MSA-P	Learning		
1.952	1.168	1.96	1.495	1.558	4.482	3.464	MSA-P	Learning		
0.048	2.211	3.014	1.463	1.029	3.983	3.082	MSA-P	Learning		

(*continued on next page*)

Table 5 (*continued*)

1HMRS	VBM z value								
NAA/Cr	cerebellum hemisphere1	cerebellum hemisphere2	MNI_Putamen_L	MNI_Putamen_R	Pons	Midbrain	Diagnosis		Prediction	Prediction %
2.46	3.215	2.986	0.033	0.108	1.657	1.083	MSA-P	Learning		
0.05	1.547	1.37	−1.014	−2.413	2.182	2.405	MSA-P	Learning		
0.309	2.157	1.517	2.289	1.614	2.327	3.104	MSA-P	Learning		
0.055	1.129	1.675	1.083	1.02	1.244	1.294	MSA-P	Learning		
0.117	1.628	1.595	1.163	1.078	1.243	1.501	MSA-P	Learning		
0.067	1.997	2.011	1.338	0.82	1.272	1.129	MSA-P	Learning		
0.059	2.441	2.853	0.436	−0.547	2.958	1.496	MSA-P	Learning		
0.246	1.182	1.073	−0.051	−1.759	1.365	1.628	PD	Learning		
0.329	0.631	0.974	0.329	0.825	1.658	1.269	PD	Learning		
0.727	1.41	1.919	−0.101	−0.267	1.481	2.528	PD	Learning		
0.074	0.581	0.201	0.605	0.417	1.201	1.053	PD	Learning		
0.095	1.309	1.827	−0.058	−0.047	1.187	1.704	PD	Learning		
0.072	0.894	1.171	1.415	1.217	1.528	3.011	PD	Learning		
1.017	0.076	0.069	1.948	1.486	0.785	0.806	PD	Learning		
0.068	1.931	2.376	−0.259	0.556	1.445	1.112	PD	Learning		
0.223	1.9	1.828	−0.712	−0.705	1.669	1.318	PD	Learning		
0.113	−0.103	0.324	−1.522	−1.631	−0.155	−0.584	normal	Learning		
0.075	1.348	0.276	0.23	0.04	0.695	1.203	normal	Learning		
0.063	−0.106	−0.361	−0.272	−0.173	1.199	1.263	normal	Learning		
0.035	−0.048	0.394	0.891	1.259	1.78	1.203	normal	Learning		
0.048	1.117	2.006	0.526	0.176	2.552	2.028	normal	Learning		
0.154	2.497	2.403	1.453	0.853	3.034	1.463		Prediction	PD	99.83%
0.132	0.377	0.308	3.068	3.593	0.244	1.721		Prediction	normal	100.00%
1.31	0.793	1	1.192	0.981	1.718	1.183		Prediction	MSA-P	82.84%
0.056	0.553	0.771	1.13	1.056	1.056	1.065		Prediction	PD	76.56%
0.068	0.473	0.714	1.553	1.985	0.568	1.033		Prediction	MSA-P	81.74%
2.08	1.5	1.648	2.534	2.239	1.853	2.275		Prediction	PD	100.00%
0.172	1.643	1.714	1.466	1.891	2.691	1.916		Prediction	MSA-P	99.59%
0.297	1.7	1.686	1.572	1.637	2.108	0.728		Prediction	MSA-P	99.94%
0.101	0.748	0.488	1.822	1.893	1.055	0.768		Prediction	normal	98.11%
0.097	0.011	0.412	1.231	1.622	0.602	1.286		Prediction	normal	69.30%

MRS, magnetic resonance spectroscopy; MSA-P, Parkinson's variant of multiple system atrophy; PD, Parkinson's disease; Lac, lactate; NAA, *N*-acetylaspartate; GABA, gamma-aminobutyric acid; Cr, creatine + phosphocreatine; Cho, choline-containing compounds; mI, myoinositol; VBM, voxel-based morphometry; MNI, an anatomical segmentation of the spatially normalized single-subject high-resolution T1 volume provided by the Montreal Neurological Institute, A z-score, one unit of standard deviation obtained using VBM (SPM 12). Learning, learning data for neural network.

peduncle atrophy, and hot cross bun sign identified using conventional MRI, which are regarded as an anomaly in MSA, are also not necessarily recognized [2,3]. These findings suggest that better and novel MRI techniques are needed to improve the sensitivity but not specificity. Therefore, new methods of distinction between MSA-P and PD are particularly important, especially in the early stages of the disease [1].

NN makes possible the prediction of the diagnosis using various types of biomarkers unlike conventional linear statistics [8,19]. We examined the clinical utilization of NN analysis using both data of VBMthat indicate the morphological changes and those of MRS that indicate the qualitative changes in intracellular metabolic status for the differential diagnosis.

VBM allows for the quantification of atrophy in regions of interest without depending on visual judgment and then can be used as an independent variable in NN, not only for various statistical analyses. Attempts have been made to differentiate between MSA-P and PD using VBM via MRI; Brenneis et al. used VBM (using SPM2) to examine morphological changes in MSA-P patients as compared with PD patients, and verified atrophy in the striatum, midbrain, thalamus, cerebellum, and various cortexes; only striatal atrophy was independent of the stage of disease [22]. Shigemoto et al. used VBM (using SPM8) to compare individuals with MSA-P and healthy individuals, and reported atrophy in the putamen, globus pallidus, cerebellum, midbrain, middle cerebellar peduncle, and pons [23]. Our VBM study (using SPM12, the latest version) involving MSA-P patients compared with PD patients revealed atrophy in the superior cerebellar peduncle, middle cerebellar peduncle, cerebellar hemisphere, putamen, pons, and midbrain. However, we did not observe significant differences in the globus pallidus. Although in the present study there were some slight differences of AAL positioning used in the VBM method and the SPM version, our findings are consistent with the results of the above-mentioned studies, except for the globus pallidus.

Since MRS can measure metabolites in the brain in vivo, it has been used for many clinical applications [10,11,17]. In the current study, we performed MRS on the globus pallidus for three reasons: 1) atrophy in the globus pallidus was not seen in either MSA or PD in our VBM study, and 2) in early PD, the changes in the globus pallidus are more pronounced on the side affected [17], and 3) at the onset of PD, the role of GABA in PD has drawn significant attention recently, and the globus pallidus is known as the important input and output area of GABA [24]. In this MRS study, changes to metabolites in the globus pallidus were observed in both PD and MSA-P (Table 3a, b). These results are consistent with those of previous studies [6,10,17]. However, there was no significant difference between the metabolic profiles of MSA-P and PD patients (Table 3c). It is thought that the observed increase in Lac indicates mitochondrial degeneration, while the increase in mI indicates gliosis, and the decrease in NAA suggests a decrease in neurons [17,18]. These results are consistent with pathological findings in MSA-P [21]. An increase of GABA in the globus pallidus that was also observed in both MSA-P and PD patients here, may indicate neuronal inhibitory dysfunction, a critical mechanism which may underlie motor dysregulation in both diseases [24]. Therefore, these findings suggested similar metabolic changes in the MSA-P as well as PD patients.

Correlation analyses were performed between the VBM and MRS data and the motor disability assessed using UMSARS-II. In this study, we failed to show a correlation of the UMSARS-II scores except for the cerebellar hemispheric region obtained with VBM. This finding may indicate that the pathological change is initiated at the beginning of disease before the emergence of clinical symptoms, and additionally, we had selected cases of the earlier stage. Brenneis et al. reported that the UPDRS-III score was not significantly correlated with any brain region in the study of MSA and PD using VBM [22].

It is a challenge to determine how to comprehensively analyze these changes and to use them to establish an appropriate diagnosis. NN approaches (also known as deep learning) have been used in various fields [8]. In the field of medicine, for example, NNs have been applied to the analysis of findings in radiology [25] and pathology [26]. We used an NN approach here because we believed that a comprehensive analysis of the various data reported in MSA-P and PD cases could only be achieved using improved potential, enabled by NN, to recognize patterns within these data.

NNs have the potential to learn complicated interrelationships within data, recognize the pattern inherent in the data by imitating the human brain function, and render predictions from the new data. They further enable the modeling of very complicated functions and solve problems that were difficult with conventional linear methods (such as linear regression and linear discriminant analysis). While various NNs can be used, we opted for a stochastic NN, often used in predicting classifications and categories [19].

The present study is characterized by the use of two types of data analyzed by an NN: VBM, which reflects morphological changes, and MRS, which reflects qualitative changes.

The differentiation between MSA-P and PD using only MRS data in the NN (MRS-NN) were unsatisfactory and the same trial with only VBM data in the NN (VBM-NN) was improved slightly; however, it exhibited low accuracy. However, in the NN including both VBM and MRS data (VBM- and MRS-NN), the accuracy of NN was fairly improved. As shown in Table 4 and Supplementary Fig. 1, the values of AUC using prediction values of NNs were 0.775 (VBM-and MRS-NN), 0.625 (VBM-NN), and 0.522 (MRS-NN).

The advantage of deep learning techniques such as NN is that one can use various data obtained using various modalities, which will help lead to better diagnosis. The methodology of this investigation using deep learning may be useful not only for clinical diagnosis of other neurodegenerative diseases but also for new findings from future studies.

In summary, our study suggests that the analysis utilizing two types of data analyzed by NN (VBM, which reflects morphological changes, and MRS, which reflects qualitative changes) can lead to better diagnosis than diagnosis using each data separately. We are aware that the small size of the data is a limitation, however, this was a pilot study. However, we believe that this methodology could improve the sensitivity of diagnosis of MSA-P. The use of a larger data set is necessary to improve the accuracy of NN-derived predictions in future studies.

5. Conclusions

In this study we used only objective MRI data, without including clinical findings, as the data for NN learning, because sometimes NN renders a diagnostic result different from the clinical diagnosis. In such cases, the NN results can provide us an opportunity to review the clinical diagnosis and neurological findings. We believe that NN is not the protagonist here; diagnoses should be rendered by the neurologist.

Declarations of interest

None.

Funding

This research did not receive any specific grant from funding agencies in the public, commercial, or not-for-profit sectors.

Acknowledgements

We thank Wada M, for help with preparing the necessary data offs this paper.

Appendix A. Supplementary data

Supplementary data to this article can be found online at https://doi.org/10.1016/j.jns.2019.04.014.

References

[1] V. Chelban, M. Bocchetta, S. Hassanein, N.A. Haridy, H. Houlden, J.D. Rohrer, An update on advances in magnetic resonance imaging of multiple system atrophy, J. Neurol. (2018 Nov 20), https://doi.org/10.1007/s00415-018-9121-3.

[2] M. Stamelou, K.P. Bhatia, Atypical parkinsonism: diagnosis and treatment, Neurol. Clin. 33 (2015) 39–56, https://doi.org/10.1016/j.ncl.2014.09.012.

[3] G. Rizzo, M. Copetti, S. Arcuti, D. Martino, A. Fontana, G. Logroscino, Accuracy of clinical diagnosis of Parkinson disease: a systematic review and meta-analysis, Neurology 86 (2016) 566–576, https://doi.org/10.1212/WNL.0000000000002350.

[4] S. Koga, N. Aoki, R.J. Uitti, J.A. van Gerpen, W.P. Cheshire, K.A. Josephs, Z.K. Wszolek, J.W. Langston, D.W. Dickson, When DLB, PD, and PSP masquerade as MSA: an autopsy study of 134 patients, Neurology 85 (2015) 404–412, https://doi.org/10.1212/WNL.0000000000001807.

[5] S. Gilman, G.K. Wenning, P.A. Low, D.J. Brooks, C.J. Mathias, J.Q. Trojanowski, N.W. Wood, C. Colosimo, A. Dürr, C.J. Fowler, H. Kaufmann, T. Klockgether, A. Lees, W. Poewe, N. Quinn, T. Revesz, D. Robertson, P. Sandroni, K. Seppi, M. Vidailhet, Second consensus statement on the diagnosis of multiple system atrophy, Neurology 71 (2008) 670–676, https://doi.org/10.1212/01.wnl.0000324625.00404.15.

[6] B. Heim, F. Krismer, R. De Marzi, K. Seppi, Magnetic resonance imaging for the diagnosis of Parkinson's disease, J. Neural Transm. 124 (2017) 915–964, https://doi.org/10.1007/s00702-017-1717-8.

[7] R.V. Oliveira, J.S. Pereira, The role of diffusion magnetic resonance imaging in Parkinson's disease and in the differential diagnosis with atypical parkinsonism, Radiol. Bras. 50 (2017) 250–257, https://doi.org/10.1590/0100-3984.2016-0073.

[8] Y. LeCun, Y. Bengio, G. Hinton, Deep learning, Nature 521 (2015) 436–444.

[9] J. Ashburner, K.J. Friston, Voxel-based morphometry-the methods, Neuroimage 11 (2000) 805–821, https://doi.org/10.1006/nimg.2000.0582.

[10] R. Ciurleo, G.D. Lorenzo, P. Bramanti, S. Marino, Magnetic resonance spectroscopy: an in vivo molecular imaging biomarker for Parkinson's disease? Biomed. Res. Int. 2014 (2014) 519816, https://doi.org/10.1155/2014/519816.

[11] U.E. Emir, P.J. Tuite, G. Öz, Elevated pontine and putamenal GABA levels in mild-moderate Parkinson disease detected by 7 tesla proton MRS, PLoS ONE 7 (2012) e30918, , https://doi.org/10.1371/journal.pone.0030918.

[12] G.K. Wenning, F. Tison, K. Seppi, C. Sampaio, A. Diem, F. Yekhlef, I. Ghorayeb, F. Ory, M. Galitzky, T. Scaravilli, M. Bozi, C. Colosimo, S. Gilman, C.W. Shults, N.P. Quinn, O. Rascol, W. Poewe, Multiple system atrophy study group, development and validation of the unified multiple system atrophy rating scale (UMSARS), Mov. Disord. 19 (2004) 1391–1402, https://doi.org/10.1002/mds.20255.

[13] C.G. Goetz, B.C. Tilley, S.R. Shaftman, G.T. Stebbins, S. Fahn, P. Martinez-Martin, W. Poewe, C. Sampaio, M.B. Stern, R. Dodel, B. Dubois, R. Holloway, J. Jankovic, J. Kulisevsky, A.E. Lang, A. Lees, S. Leurgans, P.A. LeWitt, D. Nyenhuis, C.W. Olanow, O. Rascol, A. Schrag, J.A. Teresi, J.J. van Hilten, N. LaPelle, Movement Disorder Society UPDRS revision task force., movement disorder society-sponsored revision of the unified Parkinson's disease rating scale (MDS-UPDRS): scale presentation and clinimetric testing results, Mov. Disord. 23 (2008) 2129–2170, https://doi.org/10.1002/mds.22340.

[14] M. Hoehn, M. Yahr, Parkinsonism: onset, progression and mortality, Neurology 17 (1967) 427–442, https://doi.org/10.1212/wnl.17.5.427.

[15] N. Tzourio-Mazoyer, B. Landeau, D. Papathanassiou, F. Crivello, O. Etard, N. Delcroix, B. Mazoyer, M. Joliot, Automated anatomical labeling of activations in SPM using a macroscopic anatomical parcellation of the MNI MRI single-subject brain, Neuroimage 15 (2002) 273–289, https://doi.org/10.1006/nimg.2001.0978.

[16] H. Watanabe, H. Fukatsu, M. Katsuno, M. Sugiura, K. Hamada, Y. Okada, M. Hirayama, T. Ishigaki, G. Sobue, Multiple regional 1H-MR spectroscopy in multiple system atrophy: NAA/Cr reduction in pontine base as a valuable diagnostic marker, J. Neurol. Neurosurg. Psychiatry 75 (2004) 103–109.

[17] G. Wu, Y.J. Shen, M.H. Huang, Z. Xing, Y. Liu, J. Chen, Proton MR spectroscopy for monitoring pathologic changes in the substantia nigra and globus pallidus in Parkinson disease, Am. J. Roentgenol. 206 (2016) 385–389, https://doi.org/10.2214/AJR.14.14052.

[18] M. Tsuda, S. Asano, Y. Kato, K. Murai, M. Miyazaki, A study of the globus pallidus of patients with Parkinson disease by magnetic resonance spectroscopy using artificial intelligence (neural network), Neurol. Med. 86 (2017) 628–631.

[19] A. Ruiz, P.E. L'opez-de Teruel, Nonlinear kernel-based statistical pattern analysis, IEEE Trans. Neural Netw. 12 (2001) 16–32, https://doi.org/10.1109/72.896793.

[20] C.E. Metz, Basic principles of ROC analysis, Semin. Nucl. Med. 8 (1978) 283–298.

[21] T. Ozawa, D. Paviour, P. Quinn, A. Keith, A. Josephs, H. Sangha, L. Kilford, D.G. Healy, W.N. Wood, A.J. Lees, J.L. Holton, T. Revesz, The spectrum of pathological involvement of the striatonigral and olivopontocerebellar systems in multiple system atrophy: clinicopathological correlations, Brain 127 (2004) 2657–2671, https://doi.org/10.1093/brain/awh303.

[22] C. Brenneis, K. Egge, C. Scherner, K. Seppi, M. Schocke, W. Poewe, G.K. Wenning, Progression of brain atrophy in multiple system atrophy. A longitudinal VBM study, J. Neurol. 254 (2007) 191–196, https://doi.org/10.1007/s00415-006-0325-6.

[23] Y. Shigemoto, H. Matsuda, K. Kamiya, N. Maikusa, Y. Nakata, K. Ito, M. Ota, N. Matsunaga, N. Sato, In vivo evaluation of gray and white matter volume loss in the parkinsonian variant of multiple system atrophy using SPM8 plus DARTEL for VBM, Neuroimage Clin. 2 (2013) 491–496, https://doi.org/10.1016/j.nicl.2013.03.017.

[24] L. Milosevic, R. Gramer, T.H. Kim, M. Algarni, A. Fasano, S.K. Kalia, M. Hodaie, A.M. Lozano, M.R. Popovic, W.D. Hutchison, Modulation of inhibitory plasticity in basal ganglia output nuclei of patients with Parkinson's disease, Neurobiol. Dis. 124 (2018) 46–56 (pii: S0969-9961(18)30593-X).

[25] H. Shin, K. Roberts, L. Lu, D. Demnur-Fushman, J. Yao, R. Summers, Learning to read chest-rays: recurrent neural cascade model for automated image annotation, arXiv (2016), https://doi.org/10.1109/CVPR.2016.274 1603.08486.

[26] A.A. Cruz-Roa, J.E. Ovalle, A. Madabhushi, F.A. Osorio, A deep learning architecture for image representation, visual interpretability and automated basal-cell carcinoma cancer detection, Med. Image Comput. Comput. Assist. Interv. 16 (2013) 403–410.